Chapter I: Dip-Moveout by Fourier Transform

1.1. Dip-Moveout in Theory

Consider a seismic experiment conducted over a constant-velocity subsurface having a single dipping reflector, as illustrated in Figure 1.1. As shown by Dix (1955), the traveltime t from source location s to receiver location r may be found by analyzing the triangle $s'sr$ and using the law of cosines:

$$v^2t^2 = (\overline{s'r})^2 = (\overline{ss'})^2 + (\overline{sr})^2 - 2(\overline{ss'})(\overline{sr})\cos\left(\frac{\pi}{2} + \theta\right) ,$$

where v is the constant velocity, and θ is the dip of the reflector. Note that $\overline{ss'} = 2(s - y_i)\sin\theta$, where y_i denotes the intersection (not shown) of the reflector and the surface. Simple trigonometric identities and some algebraic manipulation then yield the following expression for the traveltime t in terms of the source-receiver midpoint y and half-offset h.

$$t = \frac{2}{v}\left[(y - y_i)^2\sin^2\theta + h^2\cos^2\theta\right]^{1/2} . \qquad (1.1)$$

Define the zero-offset ($s = r = y$) traveltime to be t_0 given by

$$t_0 \equiv \frac{2}{v}(y - y_i)\sin\theta \qquad (1.2)$$

so that equation (1.1) may be rewritten as

$$t = \left(t_0^2 + \frac{4h^2\cos^2\theta}{v^2}\right)^{1/2} . \qquad (1.3)$$

Equation (1.3) is the well-known normal-moveout (NMO) equation, corrected for dip

by replacing the true velocity v with $v / \cos\theta$.

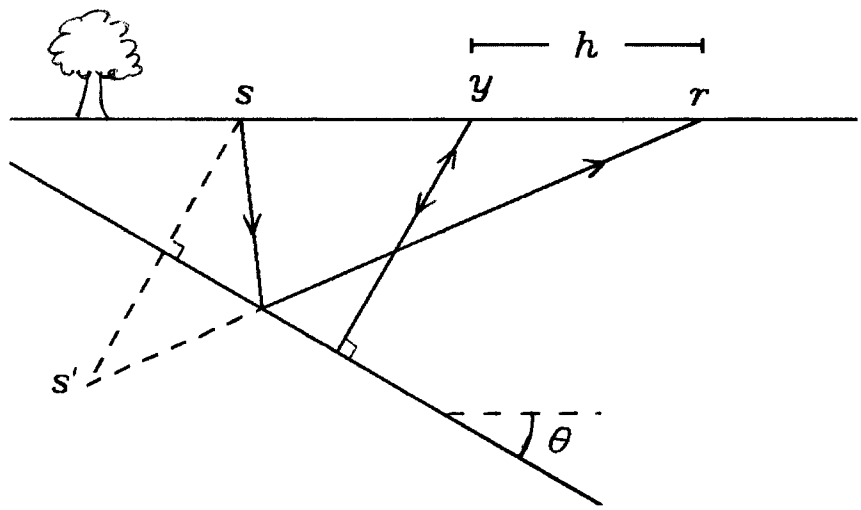

FIG. 1.1. The seismic experiment, conducted over a simplified subsurface with one dipping reflector. Applying the law of cosines to triangle $s'sr$, one may express the traveltime t from source s to receiver r in terms of zero-offset time t_0, half-offset h, velocity v, and dip θ. The result is equation (1.3) in the text, the familiar dip-corrected NMO equation.

Equation (1.3) may be used to correct for traveltime differences among seismograms recorded with different offsets. Let $p(t,y,h)$ denote seismograms (say, pressure) recorded as a function of time t, midpoint y, and half-offset h. Equation (1.3) suggests the following transformation:

$$p_0(t_0,y,h) \equiv p(\sqrt{t_0^2 + 4h^2\cos^2\theta / v^2}\,,y,h) \quad . \tag{1.4}$$

Considering only the traveltime differences among reflections recorded at different offsets (while ignoring differences due to source and receiver directivity, reflection coefficient variation with incidence angle, etc.), the function $p_0(t_0,y,h)$ defined by equation (1.4) represents zero-offset seismograms computed from non-zero-offset seismograms $p(t,y,h)$. In other words, reflections in $p_0(t_0,y,h)$ occur at the same times as reflections in the true zero-offset seismograms $p(t_0,y,h=0)$. I will refer to

the transformation defined by equation (1.4) as dip-corrected NMO.

Dip-corrected NMO may be performed as two cascaded processes. To obtain these two processes, first rewrite equation (1.3) as

$$t = \left[t_0^2 + \frac{4h^2}{v^2} - \frac{4h^2 \sin^2\theta}{v^2} \right]^{1/2} . \tag{1.5}$$

Then, define NMO time t_n (not dip-corrected) by

$$t \equiv \left[t_n^2 + \frac{4h^2}{v^2} \right]^{1/2} . \tag{1.6}$$

For equations (1.5) and (1.6) to be equivalent,

$$t_n = \left[t_0^2 - \frac{4h^2 \sin^2\theta}{v^2} \right]^{1/2} . \tag{1.7}$$

Equations (1.6) and (1.7) imply that dip-corrected NMO may be performed in two steps. Use equation (1.6) to define NMO

$$NMO \qquad p_n(t_n,y,h) \equiv p(\sqrt{t_n^2 + 4h^2/v^2},y,h) , \tag{1.8}$$

and use equation (1.7) to define dip-moveout (DMO)

$$DMO \qquad p_0(t_0,y,h) \equiv p_n(\sqrt{t_0^2 - 4h^2\sin^2\theta/v^2},y,h) . \tag{1.9}$$

Think of NMO as the transformation from recording time t to NMO time t_n; DMO is then the transformation from NMO time t_n to zero-offset time t_0.

Algebraically, the splitting of dip-corrected NMO into NMO and DMO is certainly valid; $p_0(t_0,y,h)$ computed via equations (1.8) and (1.9) equals $p_0(t_0,y,h)$ computed via equation (1.4). But, practically, why use two processes instead of one? The answer to this question is related to estimation of the velocity v. As shown below, DMO may be applied without specifying v or θ, leaving NMO as the process to use in

velocity estimation.

If one uses the correct velocity v and dip θ in applying NMO and DMO, then the *computed* zero-offset sections $p_0(t_0,y,h)$ should equal (again, considering travel-times only) the *true* zero-offset section $p(t_0,y,h=0)$ for all h. For the subsurface model of Figure 1.1, this zero-offset section is illustrated in Figure 1.2.

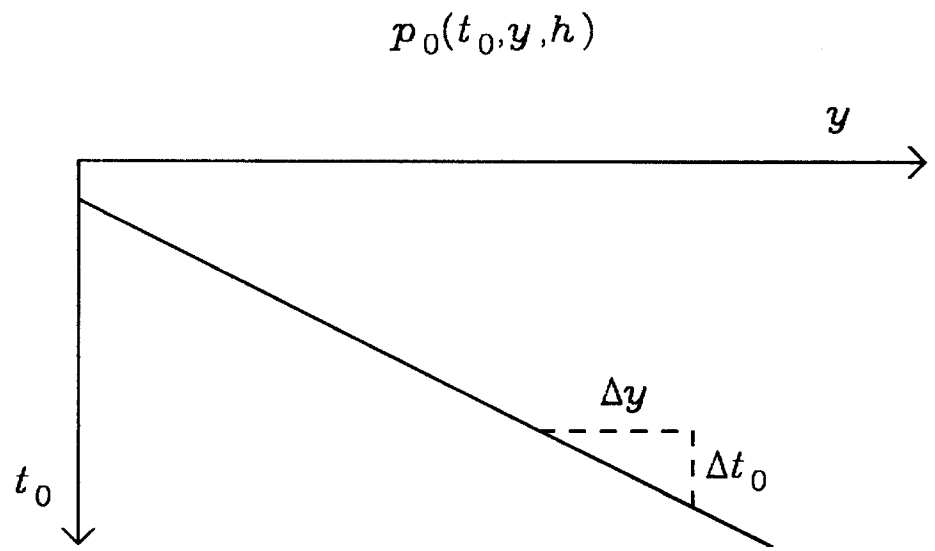

FIG. 1.2. Zero-offset section for the experiment of Figure 1.1. The slope of the reflection is $\Delta t_0/\Delta y = 2\sin\theta/v$, where θ is the dip of the reflector and v is the velocity in Figure 1.1.

From equation (1.2), the slope of the single reflection is

$$\frac{\Delta t_0}{\Delta y} = \frac{2\sin\theta}{v} ,$$

so that the DMO transformation of equation (1.9) may be expressed as

$$DMO \qquad p_0(t_0,y,h) = p_n(\sqrt{t_0^2 - (\Delta t_0/\Delta y)^2 h^2},y,h) . \tag{1.10}$$

Note that DMO via equation (1.10) does not require knowledge of the velocity v or dip θ. Because these parameters are typically unknown, equation (1.10) might seem to be preferred to equation (1.9). As a practical method of applying DMO, however,

equation (1.10) is not very useful.

DMO via equation (1.10) is impractical for two reasons. First, the slope $\Delta t_0 / \Delta y$ required for equation (1.10) to be used must be measured on a zero-offset section. Because zero-offset sections are typically not recorded, they must be computed using equations (1.8) and (1.10). To use equation (1.10), however, one needs the measured zero-offset slope.

A second and more significant problem with equation (1.10) is that more than one slope may exist at a given (t_0, y). For the simple subsurface model of Figure 1.1, only one slope is possible. Only a slightly more complex model, however, is required to illustrate the problem of conflicting slopes. Consider the subsurface model of Figure 1.3, in which the dipping reflector suddenly becomes horizontal. The zero-offset section corresponding to this model is sketched in Figure 1.4.

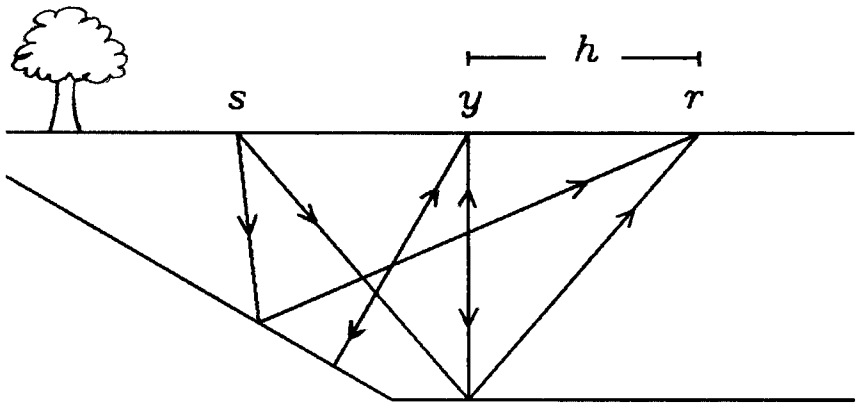

FIG. 1.3. A slightly more complicated subsurface model. The changing dip of the reflector implies that no single cosine-correction to velocity is valid for this model.

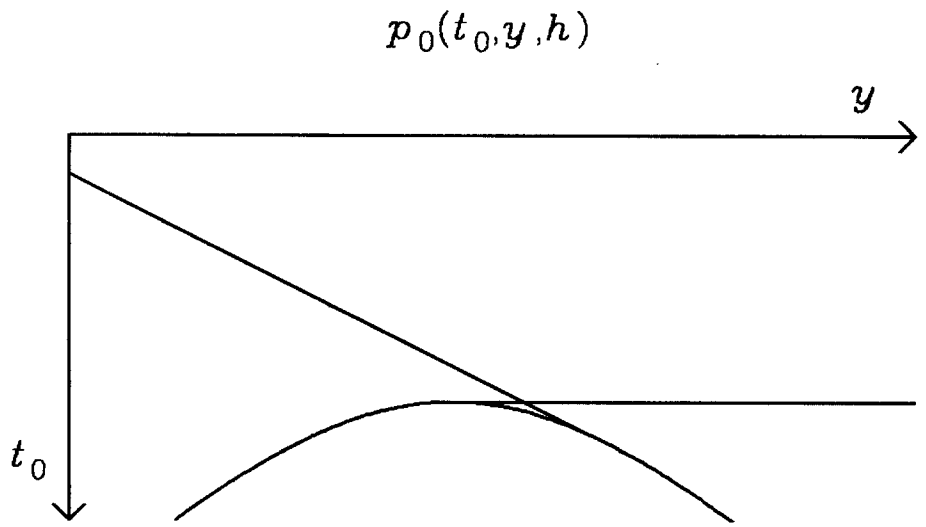

FIG. 1.4. Zero-offset section for the model of Figure 1.3, illustrating the problem of conflicting slopes. The reflection slope $\Delta t_0/\Delta y$, which varies with t_0 and y, is required to apply the dip-moveout equation (1.10) to non-zero-offset sections prior to common-midpoint (CMP) stacking. Even if one could somehow estimate, from non-zero-offset sections, the two slopes $\Delta t_0/\Delta y$ present where the reflections intersect, equation (1.10) could be applied correctly for only one slope. Hence, one slope would be enhanced relative to the other by CMP stacking.

After NMO, applying equation (1.10) with $\Delta t_0/\Delta y = 0$ to non-zero-offset sections would correctly align the horizontal reflections, while incorrectly positioning the dipping reflections. Subsequent common-midpoint (CMP) stacking (summing over h) would then attenuate the misaligned dipping reflections relative to the horizontal reflection.

Dipping reflections might be enhanced by applying equation (1.10) with $\Delta t_0/\Delta y \neq 0$, but only at the cost of attenuating the horizontal reflections in the CMP stack. Most troublesome is the point where the reflections intersect. Even if one could estimate the two distinct slopes at that point, the conventional process of stacking after dip-corrected NMO [using either equation (1.4) or equations (1.8) and (1.10)] must enhance one slope at the expense of attenuating the other. I will focus on this second problem of how to treat conflicting zero-offset slopes, for once a method to do this is found, the first problem of estimating these slopes may be eliminated by assuming that all possible slopes are present at every point (t_0,y).

Equation (1.10) implies that a different DMO correction is needed for each different zero-offset slope $\Delta t_0/\Delta y$. DMO, as the name implies, is a dip-dependent process. The two-dimensional Fourier transform (over t_0 and y) provides a particularly useful domain in which to apply a dip-dependent process, because all events having a particular slope in the (t_0,y)-domain transform to a single radial line in the (ω_0,k)-domain given by

$$\frac{k}{\omega_0} = \frac{\Delta t_0}{\Delta y} = \frac{2\sin\theta}{v} , \tag{1.11}$$

where the two-dimensional Fourier transform of $p_0(t_0,y,h)$ is defined by

$$P_0(\omega_0,k,h) \equiv \int dt_0\, e^{i\omega_0 t_0} \int dy\, e^{-iky}\, p_0(t_0,y,h) .$$

This Fourier transform may be expressed in terms of NMO-corrected data by using the following change of integration variable, which was suggested by equation (1.7):

$$t_0 = \left[t_n^2 + \frac{4h^2\sin^2\theta}{v^2}\right]^{1/2} = \left[t_n^2 + \left[\frac{\Delta t_0}{\Delta y}\right]^2 h^2\right]^{1/2} .$$

Defining

$$A \equiv \frac{dt_n}{dt_0} = \frac{t_0}{t_n} = \left[1 + \left[\frac{\Delta t_0}{\Delta y}\right]^2 \frac{h^2}{t_n^2}\right]^{1/2} ,$$

and using equation (1.10) to replace $p_0(\sqrt{t_n^2 + (\Delta t_0/\Delta y)^2 h^2},y,h) = p_n(t_n,y,h)$, the Fourier transform becomes

$$P_0(\omega_0,k,h) = \int dt_n\, A^{-1}\, e^{i\omega_0 t_n A} \int dy\, e^{-iky}\, p_n(t_n,y,h) . \tag{1.12a}$$

Using this integral transformation, which depends (through A) on the unknown zero-offset slope $\Delta t_0/\Delta y$, may seem even less practical than using the simpler equation

(1.10). But equation (1.11) implies that the unknown slope may be interpreted as the ratio k / ω_0, which suggests that A be redefined as

$$A = A(t_n,\omega_0,h,k) \equiv \left[1 + \frac{k^2h^2}{\omega_0^2 t_n^2}\right]^{1/2} . \qquad (1.12b)$$

Finally, inverse Fourier transform $P_0(\omega_0,k,h)$ to obtain the desired "zero-offset" sections $p_0(t_0,y,h)$; i.e.,

$$p_0(t_0,y,h) = \frac{1}{4\pi^2}\int d\omega_0\, e^{-i\omega_0 t_0} \int dk\, e^{iky}\, P_0(\omega_0,k,h) . \qquad (1.12c)$$

As stated earlier, the computed $p_0(t_0,y,h)$ should be interpreted as zero-offset sections only in the sense that their reflection times are the same as those in the true zero-offset section $p(t_0,y,h=0)$. This qualification bears repeating because replacing $\Delta t_0 / \Delta y$ with k / ω_0 is valid only with respect to the arrival times of reflections. A more rigorous (and considerably more complicated) analysis of the transformation from non-zero to zero offset must be based on wave theory, whereas the results in this chapter stem entirely from a geometrical analysis of raypaths. The wave-theoretical analysis is the subject of chapter III.

Equations (1.12) provide a method for applying DMO correction, not just for one slope, but for each slope $\Delta t_0 / \Delta y = k / \omega_0$ in the zero-offset section. As expected, in the limits of zero offset ($h / t_n \rightarrow 0$) and zero slope ($k / \omega_0 \rightarrow 0$), DMO does nothing. DMO correction is most significant for early reflections at large offsets ($h / t_n \rightarrow \infty$) and steep slopes ($k / \omega_0 \rightarrow \infty$).

Equation (1.12a) resembles two-dimensional Fourier transformation. The transform over y is, in fact, a Fourier transform and may be implemented digitally using any fast Fourier transform (FFT) algorithm. The transform over t_n, though not a Fourier transform, may be performed by numerically integrating over all t_n for each ω_0. Unfortunately, no fast algorithm analogous to the FFT has been found for this

transform. Some computational expense may be spared by computing $P_0(\omega_0,k,h)$ only for $k/\omega_0 \leq 2/v$. Zero-offset evanescent waves, for which $k/\omega_0 > 2/v$ (implying $\sin\theta > 1$), need not be computed when one has a lower bound for velocity v. Because h appears only as a constant parameter in equations (1.12), the data should be sorted into constant-offset sections prior to their use. DMO is most naturally applied to each constant-offset section separately.

The *DMO by Fourier transform* algorithm of equations (1.12) is, for constant velocity, accurate for all offsets and all dips. The differences between this algorithm and previously published finite-difference DMO algorithms are analogous to the differences between frequency-wavenumber (Stolt, 1978; Gazdag, 1978) and finite-difference (Claerbout, 1976) algorithms for migration. For example, just as finite-difference migration algorithms require approximations that break down at steep dips, finite-difference DMO algorithms are inaccurate for large offsets and steep dips, even for constant velocity. Although the details will be omitted here, a first step in obtaining a finite-difference implementation of equations (1.12) is to approximate the square root A in equation (1.12b) with

$$A = A(t_n,\omega_0,h,k) \approx 1 + \frac{1}{2}\frac{k^2h^2}{\omega_0^2 t_n^2} .$$

(Compare this approximation, for example, with that made by Bolondi et al, 1982.) Additional approximations are required to represent partial derivatives with finite-difference operators.

Accuracy, of course, is not the only important consideration in choosing an algorithm. The ability to cope with finite computational grid boundaries is also important. Whereas finite-difference algorithms are made to handle this problem rather easily, frequency-wavenumber algorithms are not. And in practice, one also considers factors such as the cost and complexity of an algorithm (factors that, unlike accuracy, depend on available computer hardware). One should also consider the way in which

an algorithm fits into the total processing sequence, and this practical consideration is the subject of the following section.

1.2. Dip-Moveout in Practice

Figures 1.5 illustrate the correct processing sequence including DMO. In Figure 1.5a is plotted a synthetic constant-offset section containing only eight non-zero samples. While it is unlikely that this synthetic section would actually be recorded, it serves to illustrate the time-variable impulse response of the entire processing sequence. Furthermore, geometrical optics predicts that this non-zero-offset section will correspond to an earth with elliptical reflectors buried in the subsurface. Specifically, if $p(t,y,h)$ contains impulses at points (t_p,y_p), then the corresponding subsurface ellipses are given by

$$\frac{(y-y_p)^2}{\left(\frac{v^2 t_p^2}{4}\right)} + \frac{t_m^2}{\left(t_p^2 - \frac{4h^2}{v^2}\right)} = 1 \ ,$$

where t_m is migrated (two-way vertical) time defined by $t_m \equiv 2z/v$, with z denoting depth. (See, for example, Deregowski and Rocca, 1981.) Correct processing of the section plotted in Figure 1.5a should yield images of these elliptical reflectors.

Figure 1.5b is the result of applying NMO, the prerequisite to DMO, to the data of Figure 1.5a, assuming a constant velocity of 2 km/sec. Applying DMO via a discrete implementation of equations (1.12) then yields the zero-offset section plotted in Figure 1.5c. $P_0(\omega_0,k,h)$ was computed for all ω_0 and k; in particular, evanescent waves were not zeroed. Because the velocity for this synthetic test was assumed to be v = 2 km/sec, all slopes in Figure 1.5c greater that 1 sec/km represent evanescent waves which are zeroed by migration.

Figure 1.5d, obtained by migrating the zero-offset section of Figure 1.5c, verifies the ray-theoretical prediction that the constant-offset section in Figure 1.5a corresponds to a subsurface containing semielliptical reflectors. (The reader should check the lengths of the major and minor axes and draw the corresponding raypaths.) Had DMO not been applied, the reflectors in Figure 1.5d would have incorrectly appeared semicircular. Figure 1.5d confirms that DMO correction via equations (1.12) is accurate with respect to traveltime. The wave-theoretical analysis of chapter III is required to judge the amplitude variations with dip seen in Figures 1.5c and 1.5d.

Recall that, except for the optional dip filtering of evanescent waves, DMO via equations (1.12) is velocity-independent; no unknown parameters are required to perform DMO. In computing the zero-offset section of Figure 1.5c, the velocity v was used only in the NMO process. Remember, however, that the derivation of equations (1.12) is correct only for a constant velocity v. In practice, the assumption that velocity is constant cannot be made in processing recorded seismic data. And, although I know of no exact generalization of equations (1.12) for variable velocity, any attempt to approximately handle velocity variations must make the DMO process velocity-dependent (e.g., Yilmaz and Claerbout, 1980; Deregowski and Rocca, 1981).

A velocity-dependent generalization of equations (1.12) to approximately treat depth-variable velocity is the subject of chapter II. There I demonstrate that the difference between ignoring and honoring velocity variations in DMO correction may often be negligible. If one thinks of DMO correction as a first-order correction to conventional NMO and stack, then coping with velocity variations in DMO is a second-order correction. In practice, the prerequisite estimation of velocity for NMO correction and poststack migration is the more significant problem. In this chapter, I assume that velocity variations need be considered only in applying the latter two processes.

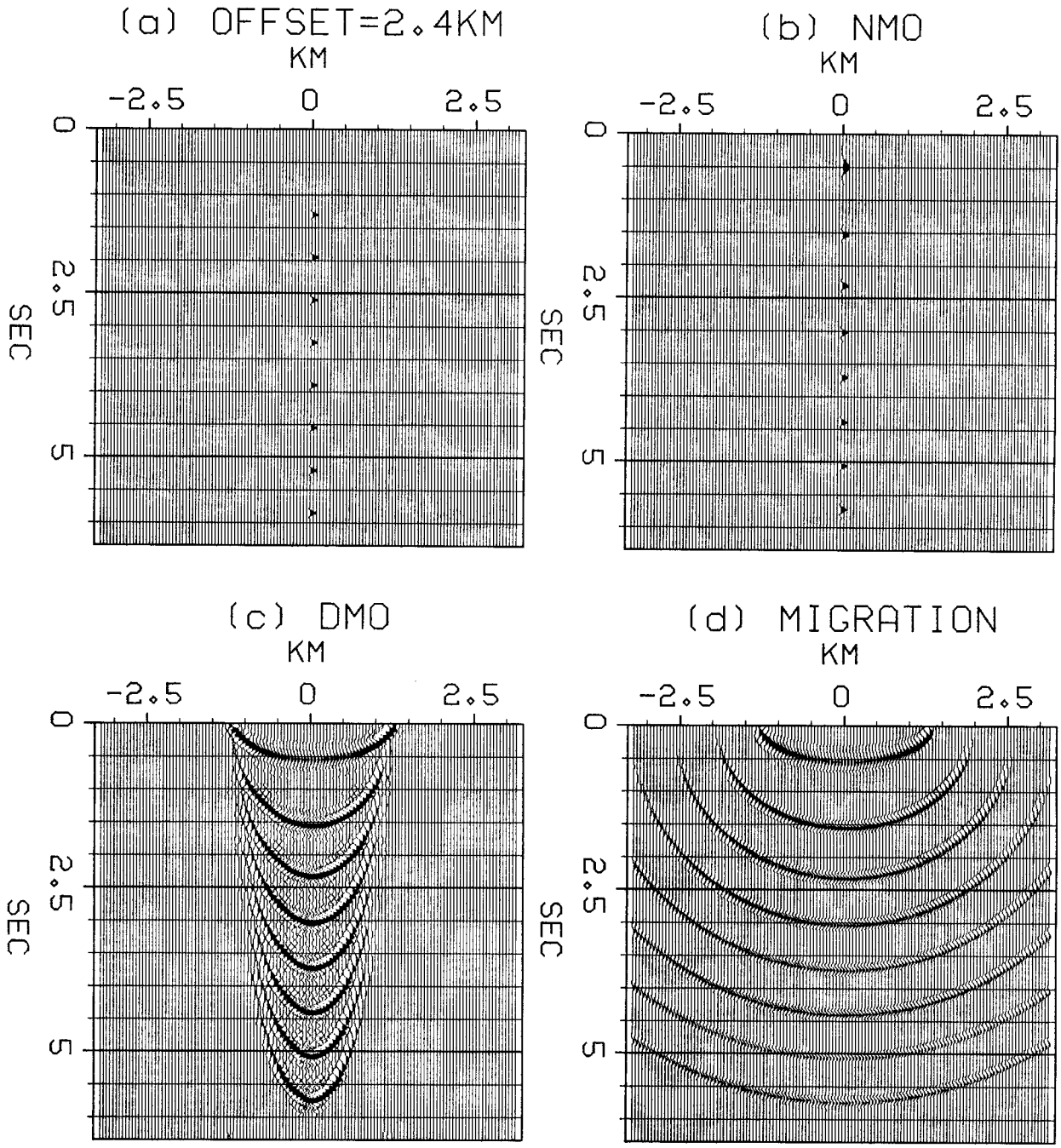

FIG. 1.5. The correct processing sequence including DMO: (a) a synthetic constant-offset section consisting of eight impulses; (b) after applying NMO with velocity v = 2 km/sec; (c) after applying velocity-independent DMO using equations (1.12); (d) after migrating with velocity v = 2 km/sec. Note the correct semielliptical shape of the reflectors; had DMO not been included in this sequence, the reflectors would have appeared semicircular. Normally, if more than one offset were recorded, the constant-offset sections would be stacked after DMO. The plotting gain in (c) and (d) is ten times that in (a) and (b).

Velocity is usually estimated by computing some measure of similarity, say, semblance, among the NMO-corrected seismograms $p_n(t_n,y,h)$ that comprise a common-midpoint gather. Semblance is computed for many different trial velocities and, when DMO correction is insignificant, the velocity yielding the highest semblance should equal, to a good approximation, the root-mean-square (RMS) velocity for a particular t_n and y (Taner and Koehler, 1969). But, if DMO correction is significant, then the discussion of the previous section 1.1 implies that semblance should not be computed from the $p_n(t_n,y,h)$, but rather from the NMO- and DMO-corrected seismograms $p_0(t_0,y,h)$. So theoretically, to estimate velocity, one must perform NMO and DMO for many different velocities. But practically, because DMO is relatively expensive compared to NMO, one would rather perform (1) velocity-independent DMO, followed by (2) conventional velocity analysis based on NMO for many trial velocities, followed by (3) NMO and stack. This preferred processing sequence should be modified, however, because theoretically NMO must precede DMO.

Unfortunately, NMO and DMO do not commute, as demonstrated in Figures 1.6. Figures 1.6 were computed using the same processes used in computing Figures 1.5, but with DMO performed before NMO as in the preferred processing sequence. The differences between Figures 1.5c and 1.6c (and the differences between Figures 1.5d and 1.6d) are most significant at early times and steep dips, for which DMO is most important.

A practical way to reduce the error in assuming that NMO and DMO commute is to apply (1) approximate NMO (ANMO) based on an initial estimate v_a of the true velocity v, followed by (2) DMO, and then (3) residual NMO (RNMO). Conceptually, RNMO may be thought of as inverse NMO using v_a, followed by NMO using v. The theoretically correct process is to apply (1) ANMO, followed by (2) RNMO, followed by (3) DMO. If the RNMO correction is small, then it approximately commutes with DMO, so that the practical process of applying DMO before velocity analysis and RNMO is

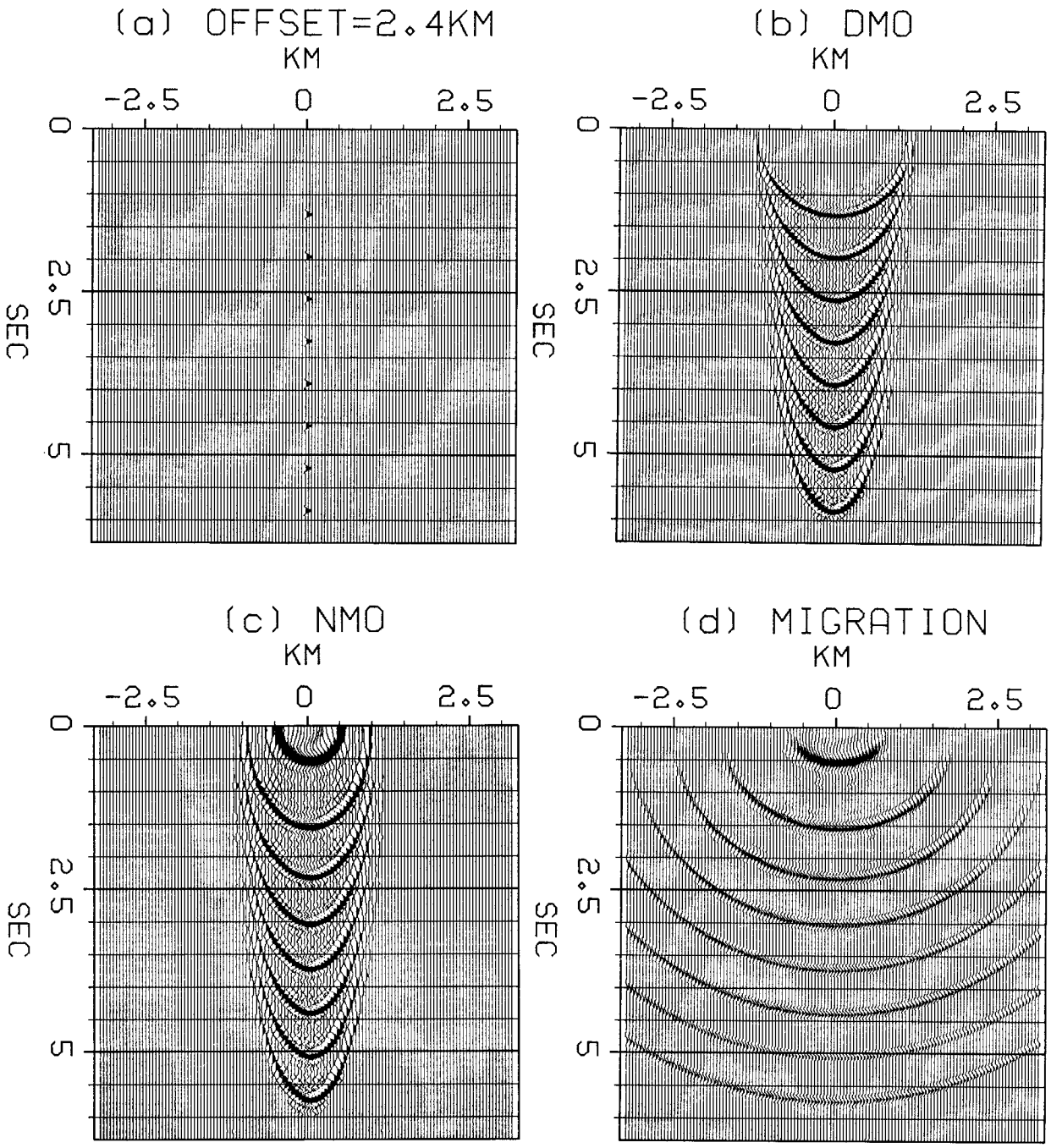

FIG. 1.6. A practical, but incorrect, processing sequence: (a) a synthetic constant-offset section consisting of eight impulses; (b) after applying velocity-independent DMO using equations (1.12); (c) after applying NMO with velocity v = 2 km/sec; (d) after migrating with velocity v = 2 km/sec. Compare Figures 1.6c and 1.6d with Figures 1.5c and 1.5d. Ideally, DMO should be performed after NMO; but in estimating velocity, DMO would likely be applied before NMO. The plotting gain in (b), (c), and (d) is ten times that in (a).

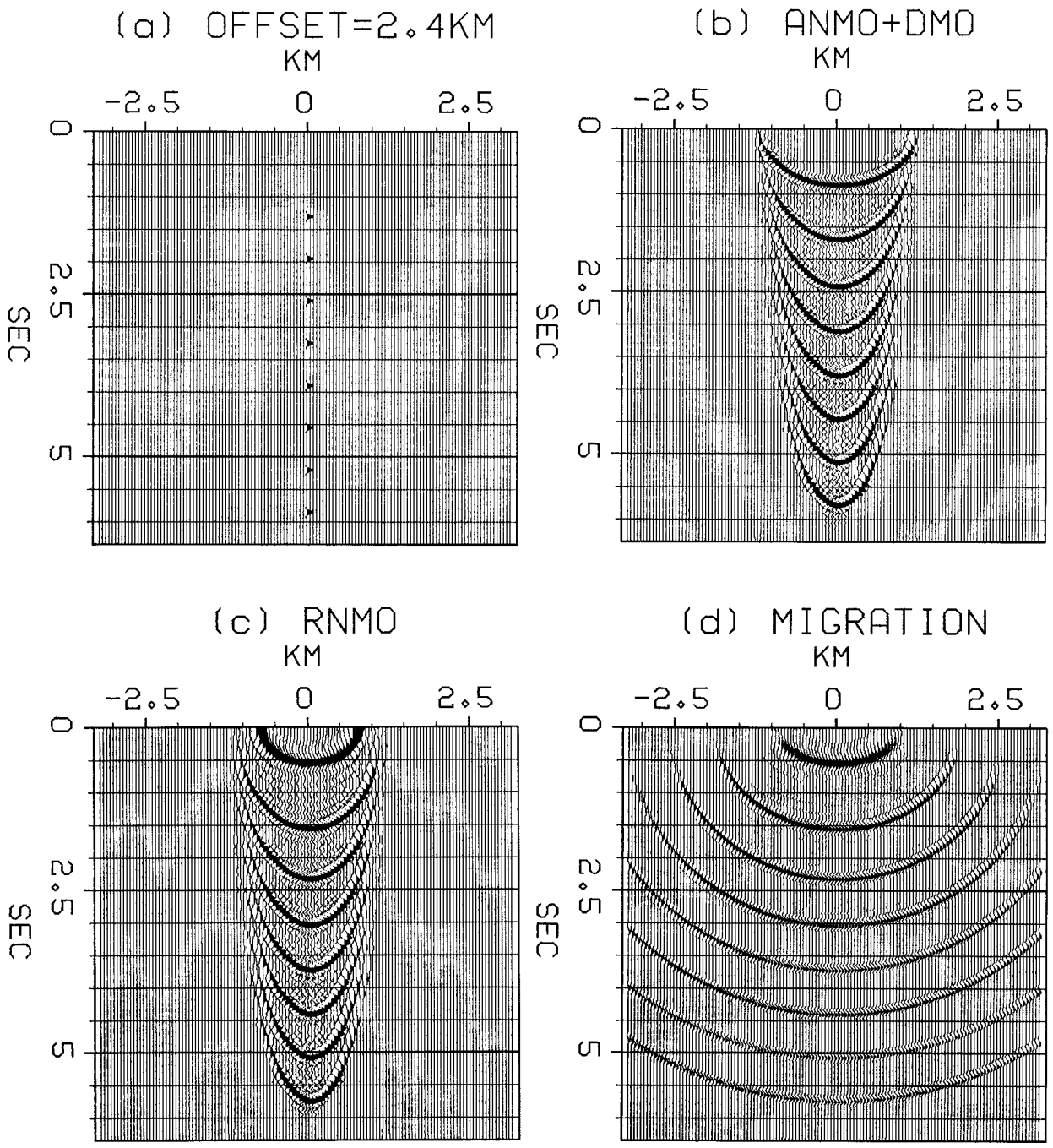

FIG. 1.7. A practical and reasonably accurate processing sequence: (a) a synthetic constant-offset section consisting of eight impulses; (b) after applying approximate NMO with velocity v_a = 2.4 km/sec followed by DMO using equations (1.12); (c) after applying residual NMO; (d) after migrating with velocity v = 2 km/sec. The relatively small residual NMO correction approximately commutes with DMO. Compare Figures 1.5c, 1.6c, and 1.7c, as well as Figures 1.5d, 1.6d, and 1.7d. The plotting gain in (b), (c), and (d) is ten times that in (a).

reasonably accurate.

Figures 1.7 illustrate this practical processing method. The section plotted in Figure 1.7b was computed by applying ANMO using a velocity v_a = 2.4 km/sec, followed by DMO. Figure 1.7c was computed by applying RNMO to the section of Figure 1.7b. Comparing Figure 1.7c with the correct Figure 1.5c and the incorrect Figure 1.6c reveals that the practical process with only RNMO after DMO is better than performing all NMO after DMO.

Comparison of the migrated sections in Figures 1.5d, 1.6d, and 1.7d indicates that the differences between these sections are slight for all but the shallowest reflectors. In deciding whether to apply NMO before or after DMO, remember that seismograms are typically muted (zeroed) for large h/t_n. If the constant-offset section in Figure 1.5a were real seismic data, the earliest reflection would likely be muted due to the excessive NMO stretch seen in Figure 1.5b. Therefore, in comparing Figures 1.5c, 1.6c, and 1.7c, little practical significance should be given to the differences in the earliest reflection.

This discussion regarding the practical aspects of DMO can be summarized as follows:

1. If velocities must be estimated, then DMO is most practically applied before velocity analysis and NMO.
2. Although DMO should theoretically be applied after NMO, DMO may be applied before NMO without significant loss of accuracy.
3. Accuracy may be improved by applying approximate NMO prior to DMO, followed by velocity analysis and residual NMO.

The following example of DMO applied to recorded seismic data further emphasizes these practical considerations.

1.3. Dip-Moveout Applied to Seismic Data

After examining the theoretical and practical aspects of DMO, the reader may appreciate an example of its application to recorded seismograms. To illustrate the effects of including DMO in the processing sequence, the data in this example were processed with and without DMO. DMO was included in the processing sequence used to compute the migrated CMP stack plotted in Figure 1.8a, whereas DMO was omitted in the processing sequence used to compute the section of Figure 1.8b. Except for including or omitting DMO, the processing sequences used to compute these two figures were identical. A detailed discussion of the DMO processing sequence is provided at the end of this section.

The differences between the two sections are most apparent near the steeply dipping fault planes. Whereas reflections from the fault planes are visible after processing which includes DMO, these reflections are attenuated when DMO is omitted from the processing sequence. Generally, the section in Figure 1.8a has a higher dip bandwidth than the section in Figure 1.8b.

As one might expect, most of the steeply dipping images of the fault planes in Figure 1.8a are well aligned with discontinuities in the almost horizontal reflectors. Fault-plane reflections and discontinuous horizontal reflections both help to locate the faults in the migrated CMP stack. An exception, however, is the steeply dipping reflection at about 2.0 seconds near CMP 370, which does not coincide with any apparent discontinuity in the horizontal reflections. An untested hypothesis to explain this inconsistency is that the steeply dipping reflection is due to a fault plane having a strike that is not perpendicular to the survey line. Three-dimensional recording and processing would provide a test of this hypothesis.

To highlight the differences between processing with and without DMO, the section in Figure 1.8b was subtracted from the section in Figure 1.8a to obtain the difference section plotted in Figure 1.8c. Note that the differences are most

significant, as expected, for the steeply dipping events; DMO does nothing to horizontal reflections. (The apparently horizontal shallow event, which actually has a very high spatial frequency, is due to the normal fluctuation of offsets with CMP when source and receiver spacings are equal in recording.) In this example, most of the differences between processing with and without DMO lie near the fault planes and along the salt contact (lower right), commonly the areas that are most interesting to the explorationist. The central portions of Figures 1.8 are replotted with an expanded scale in Figures 1.9.

The differences between the migrated sections plotted in Figures 1.8a and 1.8b may, of course, be traced to differences in the unmigrated CMP stacks. The CMP stacks that were migrated to obtain Figures 1.8a and 1.8b are plotted in Figures 1.10a and 1.10b, respectively. The difference in the stacks is plotted in Figure 1.10c. Again, the major differences are in reflections having steep slopes. The fault-plane reflections preserved in Figure 1.10a by DMO processing are attenuated in Figure 1.10b, for which DMO was omitted from the processing sequence. The central portions of Figures 1.10 are replotted with an expanded scale in Figures 1.11.

In addition to enhancing dip bandwidth (or resolution) in stacked sections, DMO may favorably influence prestack processing, particularly velocity estimation. The CMP gathers plotted in Figures 1.12a and 1.12b contain the seismograms that were stacked to obtain the CMP 100 traces plotted in Figures 1.10a and 1.10b, respectively. NMO correction appears to have aligned most of the reflections in these gathers quite well. Close inspection of Figures 1.12a and 1.12b, however, reveals a strong reflection at approximately 2.3 sec that is well aligned in Figure 1.12a but poorly aligned in Figure 1.12b. And, as one might expect, Figure 1.10c indicates that DMO significantly affects the CMP 100 stack at about 2.3 sec. The misaligned reflection in Figure 1.12b is a reflection from a steeply dipping fault plane; this reflection is attenuated by CMP stacking. DMO correction ensures that this

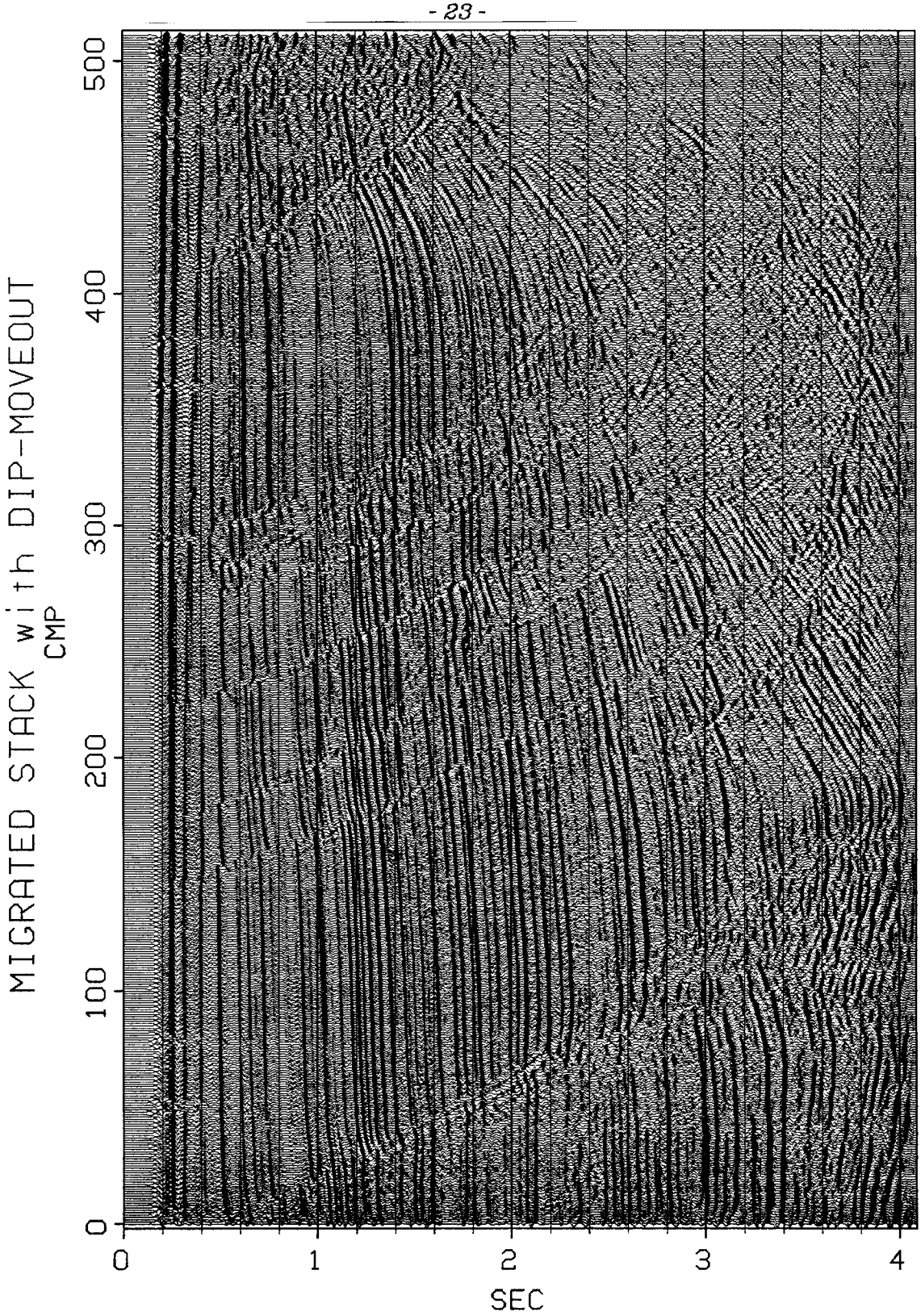

FIG. 1.8a. Migrated CMP stack of DMO- and NMO-corrected data. Notice the steeply dipping reflections from the fault planes; these reflections are not filtered by CMP stacking because DMO was included in the processing sequence. Compare this section with that in Figure 1.8b, for which DMO was omitted from the processing sequence. The CMP interval is 0.033 km.

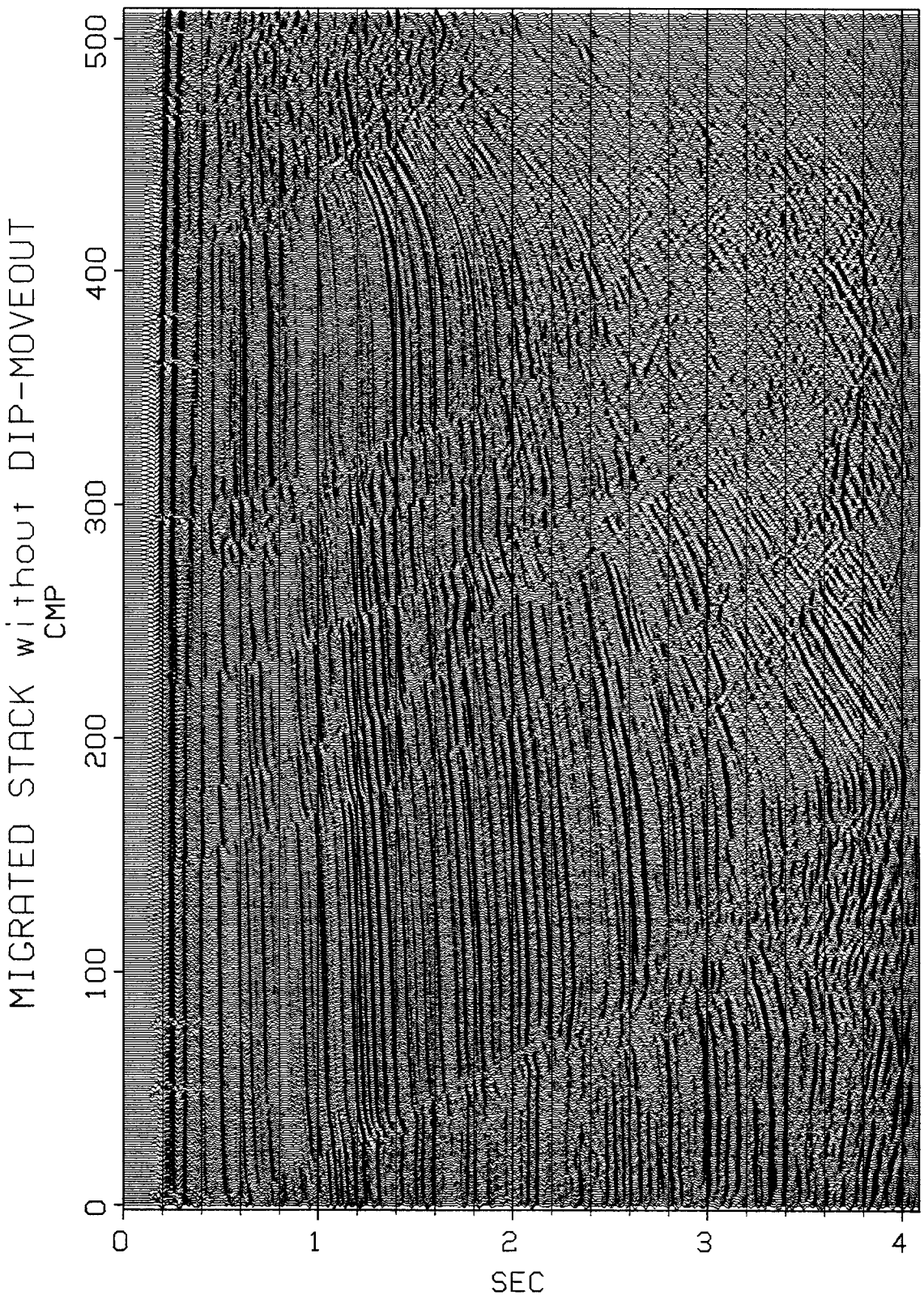

FIG. 1.8b. Migrated CMP stack of NMO-corrected data. DMO was not applied in computing this section. The steeply dipping fault-plane reflections seen in Figure 1.8a are not apparent in this figure; these reflections were attenuated by CMP stacking because DMO was omitted from the processing sequence. The CMP interval is 0.033 km.

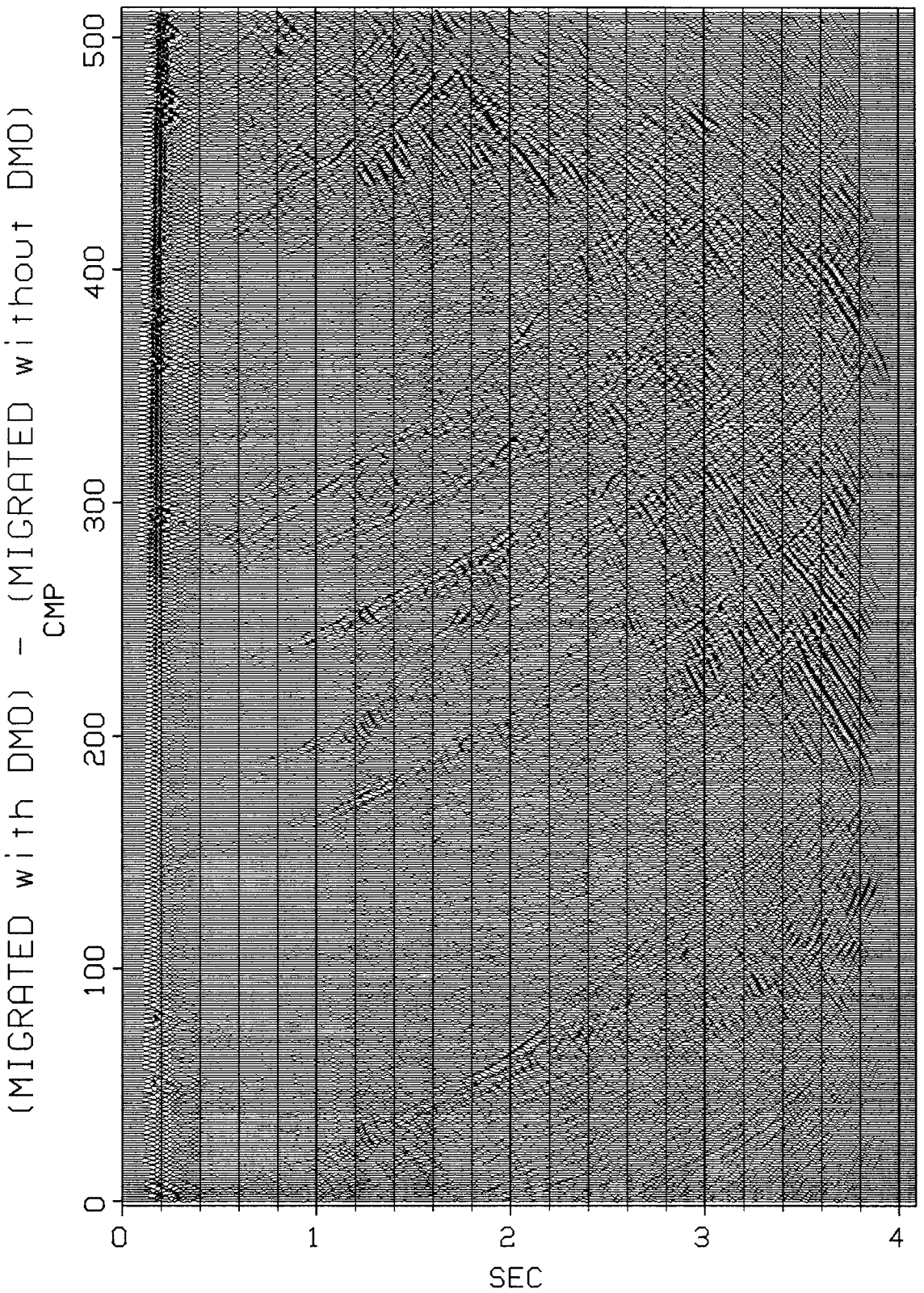

FIG. 1.8c. Figure 1.8b subtracted from Figure 1.8a; i.e., the difference between including or omitting DMO in the processing sequence. Horizontal reflections are clearly not affected by DMO. The most significant differences lie near the fault planes and along the salt contact, commonly the areas that are most interesting to the explorationist. Figures 1.8a, 1.8b, and 1.8c are all plotted with the same gain.

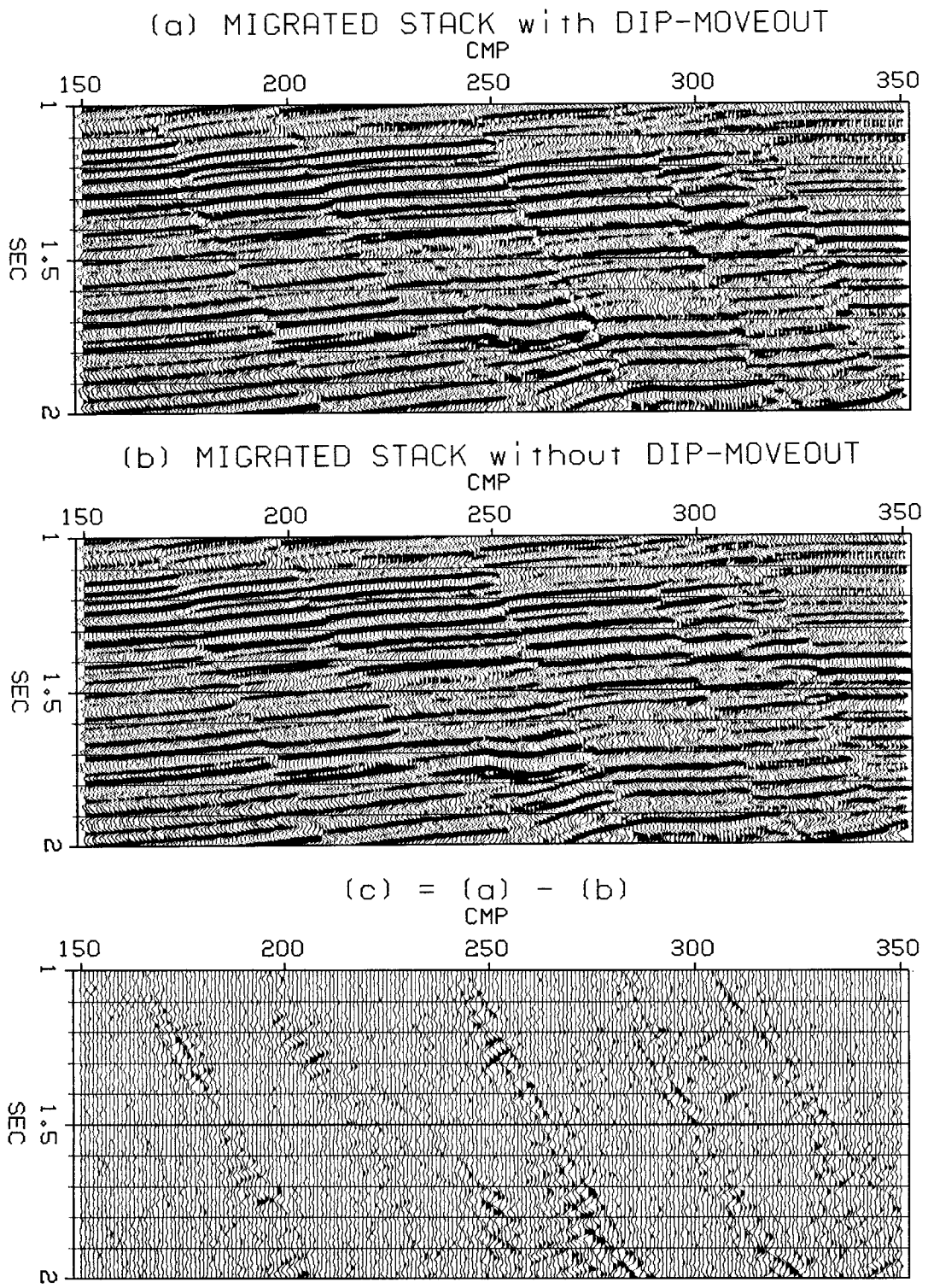

FIG. 1.9. The central portions of Figures 1.8a, 1.8b, and 1.8c replotted with an expanded scale.

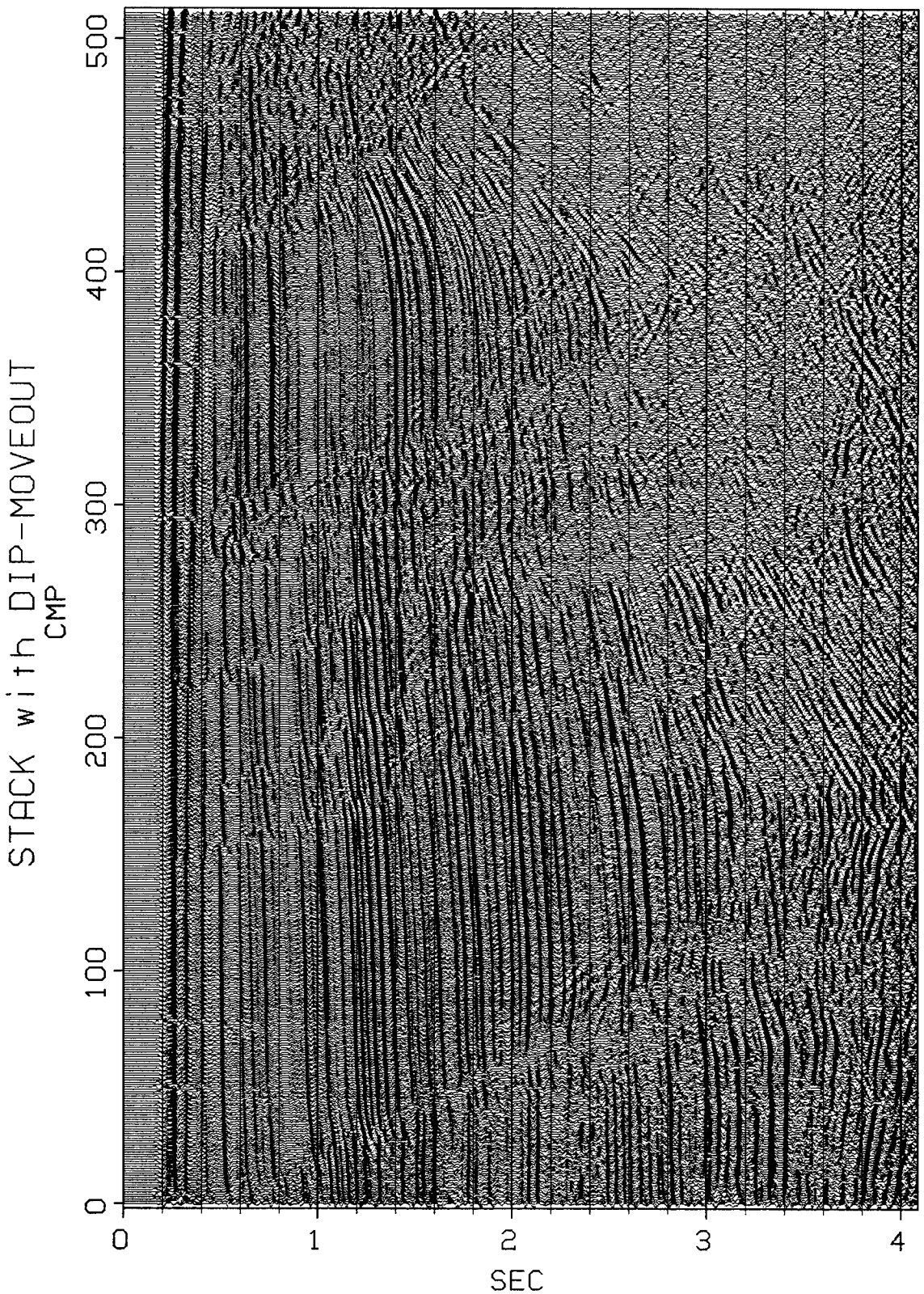

FIG. 1.10a. CMP stack of DMO- and NMO-corrected data. This section was migrated to obtain the section plotted in Figure 1.8a. Compare this section with that of Figure 1.10b to verify that DMO enhances the dip bandwidth of the CMP stack. The CMP interval is 0.033 km.

FIG. 1.10b. CMP stack of NMO-corrected data. DMO was not applied in computing this section. This stack was migrated to obtain the section plotted in Figure 1.8b. Compare this section with that of Figure 1.10a to verify that omitting DMO from the processing sequence degrades the dip bandwidth of the CMP stack. The CMP interval is 0.033 km.

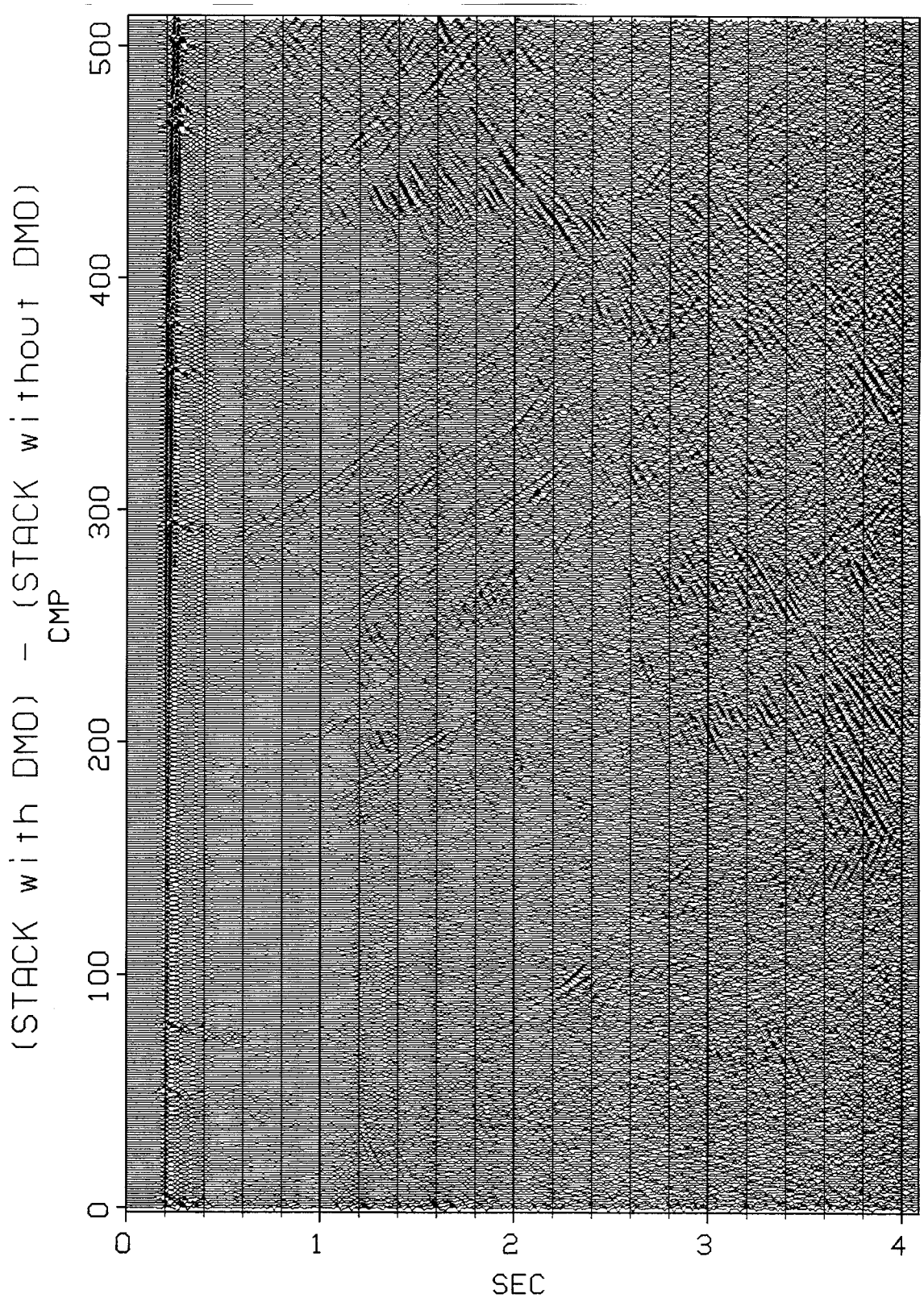

FIG. 1.10c. Figure 1.10b subtracted from Figure 1.10a; i.e., the difference between including or omitting DMO in the processing sequence. As in Figure 1.8c, the major differences are in reflections having steep slopes. Figures 1.10a, 1.10b, and 1.10c are all plotted with the same gain.

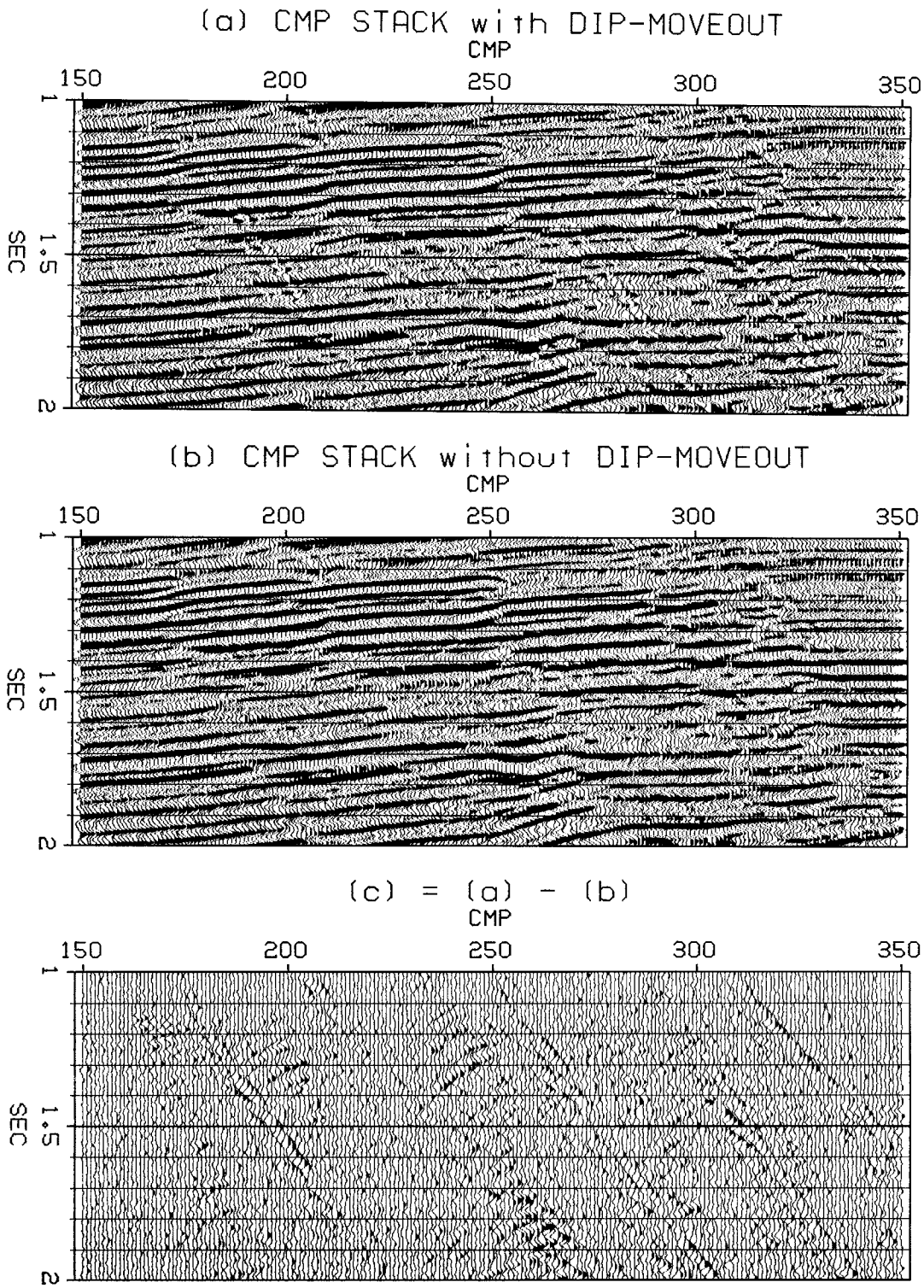

FIG. 1.11. The central portions of Figures 1.10a, 1.10b, and 1.10c replotted with an expanded scale.

reflection is well aligned and, therefore, enhanced by CMP stacking of the traces in Figure 1.12a.

At the expense of attenuating horizontal reflections, the misaligned reflection in Figure 1.12b can be aligned without applying DMO simply by using a higher NMO velocity. A conventional velocity analysis, in which semblance between NMO-corrected seismograms is computed for many trial velocities, confirms this fact. Contoured in Figures 1.13a and 1.13b are the semblances for the CMP 100 gathers processed with and without DMO, respectively. No experienced interpreter would "pick" the anomalously high velocity corresponding to the semblance peak at 2.3 sec in Figure 1.13b. This anomalous peak is absent in Figure 1.13a, because DMO enables reflections with conflicting slopes to be stacked at the same velocity.

The NMO velocities used in computing the CMP stacks of Figures 1.10a and 1.10b were, in both cases, those estimated from the DMO-corrected CMP gathers. In particular, when computing the stack of Figure 1.10b, I did not use velocity estimates obtained from the data that was not DMO-corrected. Therefore, the stack in Figure 1.10b does not quite represent "conventional" processing. The use of different velocities in stacking the data with and without DMO would have made an objective comparison of figures such as 1.10a and 1.10b impossible, due to the subjectivity involved in picking velocities from contoured semblances.

DMO processing of the data in the examples above was performed using the approximate but practical sequence of approximate NMO, followed by DMO, followed by residual NMO. The details of the DMO processing sequence are as follows:

1. An initial estimate of velocity was obtained by first contouring semblance, as in Figures 1.13, and then picking a time-dependent velocity function for six uniformly spaced CMPs.

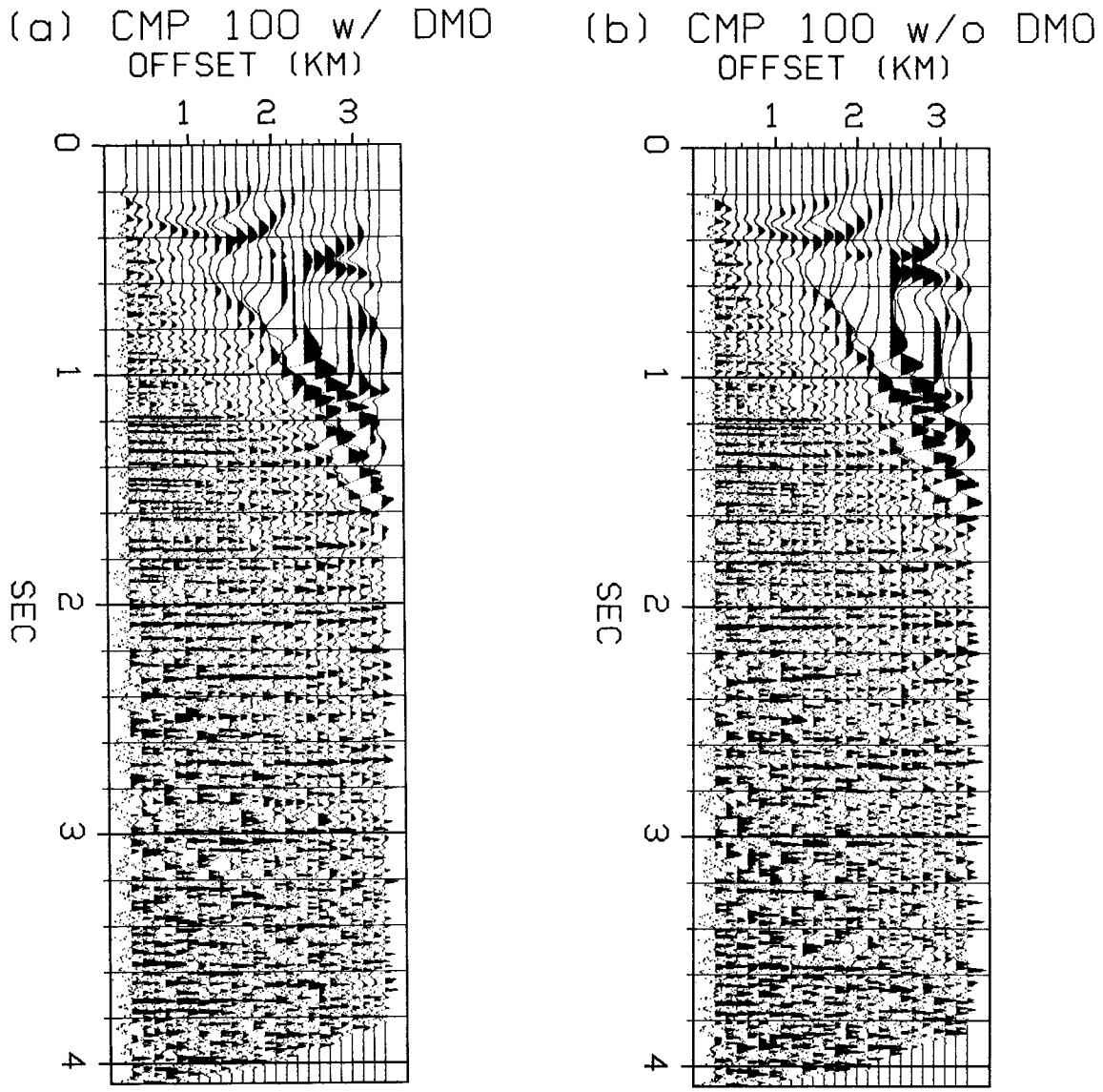

FIG. 1.12. (a) The CMP gather that was stacked to obtain the trace at CMP 100 plotted in Figure 1.10a. (b) The CMP gather that was stacked to obtain the trace at CMP 100 plotted in Figure 1.10b. The reflection at about 2.3 sec, which is well aligned in (a) but misaligned in (b), is a reflection from a steeply dipping fault plane. This reflection is preserved in stacking gather (a), for which DMO was applied, but attenuated in stacking gather (b), for which DMO was omitted. Data for which NMO stretch is excessive are zeroed prior to stacking.

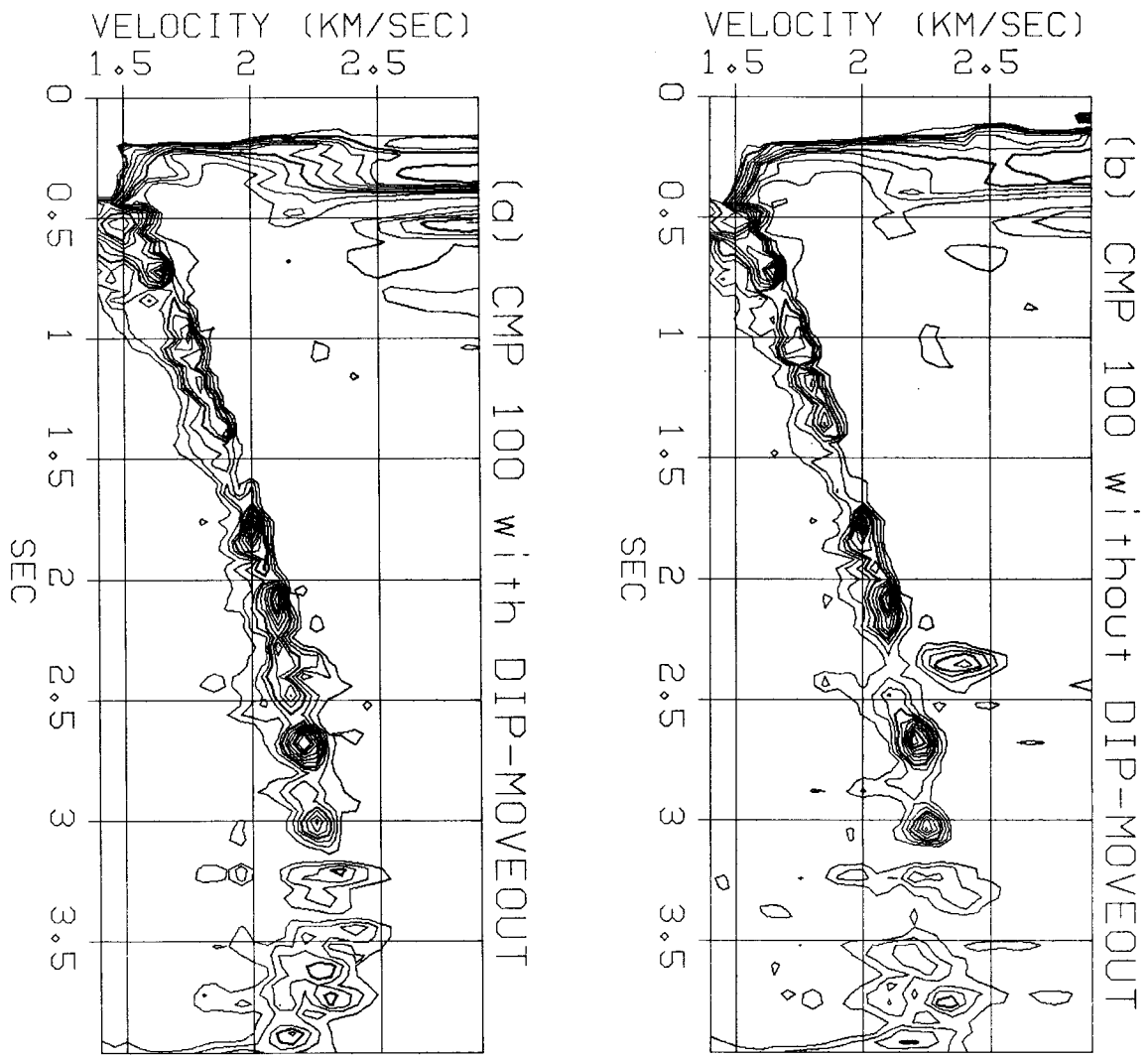

FIG. 1.13. (a) Velocity analysis for the DMO- and NMO-corrected CMP 100 gather plotted in Figure 1.12a. (b) Velocity analysis for the NMO-corrected CMP 100 gather plotted in Figure 1.12b. In Figure 1.13b, the anomalously high velocity corresponding to the semblance peak at 2.3 sec is due to a steeply sloping fault plane reflection. This peak is absent in Figure 1.13a, because DMO enables reflections with conflicting slopes to be stacked with the same velocity. Normalized semblance is contoured at intervals of 0.05; bold contours represent semblance values of 0.25 and 0.5.

2. Using the average of the six velocity functions obtained in step 1., NMO correction was applied to each CMP gather.

3. DMO correction was applied by sorting the data into constant-offset sections, applying a discrete implementation of equations (1.12) to each constant-offset section, and then re-sorting the data into CMP gathers.

4. The NMO correction applied in step 2. was removed. Velocities were estimated as in step 1., except that here the DMO-corrected CMP gathers were used.

5. NMO correction and stacking was performed using the time- and midpoint-dependent velocity function estimated in step 4.

6. The CMP stack was migrated using the phase-shift algorithm described by Gazdag (1978).

Some steps may bear further discussion. First, as discussed in section 1.2, the initial NMO correction in step 2. improves the accuracy of the practical processing sequence, leaving only a small residual NMO correction that approximately commutes with DMO. Second, because source and receiver spacings were equal in recording, the offset in each constant-offset section in step 3. actually fluctuated with CMP number. In a near-offset section, for example, the offset for even-numbered CMPs was 0.262 km; for odd-numbered CMPs, the smallest offset was 0.329 km. The average of two such offsets was used in DMO correction of each "constant-offset" section. Third, the inverse-NMO correction applied in step 4. may be omitted if one interprets subsequent velocity analysis and NMO correction as residual processes. Inverse-NMO was used here to make comparisons such as the one in Figures 1.13 possible. And fourth, lateral velocity variations were considered too small to warrant the use of a more accurate and elaborate migration algorithm than that used in step 6.

1.4. Summary

Dip-moveout by Fourier transform is defined by the following equations:

$$P_0(\omega_0,k,h) \equiv \int dt_n \; A^{-1} \; e^{i\omega_0 t_n A} \int dy \; e^{-iky} \; p_n(t_n,y,h) \qquad (1.12a)$$

$$A = A(t_n,\omega_0,h,k) \equiv \left[1 + \frac{k^2h^2}{\omega_0^2 t_n^2}\right]^{1/2} \qquad (1.12b)$$

$$p_0(t_0,y,h) = \frac{1}{4\pi^2} \int d\omega_0 \; e^{-i\omega_0 t_0} \int dk \; e^{iky} \; P_0(\omega_0,k,h) \; . \qquad (1.12c)$$

This DMO algorithm enables the computation of zero-offset seismograms $p_0(t_0,y,h)$ from NMO-corrected seismograms $p_n(t_n,y,h)$; and, if velocity is constant, the algorithm is accurate (with respect to traveltimes) for all offsets and all reflector dips. In practice, some accuracy is lost because (1) velocity is never constant and (2) DMO will likely be performed before NMO in estimating velocity. Nevertheless, DMO by Fourier transform compares favorably with even less accurate finite-difference DMO algorithms.

Application of DMO permits reflections having different zero-offset slopes to stack coherently with the same NMO velocity, thereby (1) reducing the dip-filtering action of conventional NMO and stack and (2) improving velocity estimates. The example in section 1.3 of DMO applied to recorded seismograms illustrates that these two advantages of DMO processing are most significant near regions of spatial discontinuity, typically the regions most interesting to the explorationist.